J Gastric Cancer. 2026 Apr;26(2):260-278
https://doi.org/10.5230/jgc.2026.26.e19
pISSN 2093-582X·eISSN 2093-5641

jgc Journal of Gastric Cancer

Original Article

Check for updates

Molecular and Phenotypic Characterization of Fluid-Derived Patient-Derived Cell and Organoid Models in Advanced Gastric Cancer

Ye Jin Moon [1,2], **Woo Sun Kwon** [1], **Chan Hee Park** [1], **Jinsoo Jang** [1], **Juin Park** [1,3], **Byeong Gyu Yoon** [1,3], **Han Byeol Mun** [1,2], **Namju Kim** [1], **Choong-kun Lee** [1,4], **Hei Cheul Jeung** [1,5], **Su-Jin Shin** [6], **Tae Soo Kim** [1], **Sun Young Rha** [1,2,3,4]

[1]Song-Dang Institute for Cancer Research, Yonsei University College of Medicine, Seoul, Korea
[2]Brain Korea 21 Project, Graduate School of Medical Science, Yonsei University College of Medicine, Seoul, Korea
[3]Department of Medicine, Yonsei University College of Medicine, Seoul, Korea
[4]Division of Medical Oncology, Department of Internal Medicine, Yonsei Cancer Center, Yonsei University College of Medicine, Seoul, Korea
[5]Department of Internal Medicine, Gangnam Severance Hospital, Yonsei University College of Medicine, Seoul, Korea
[6]Department of Pathology, Gangnam Severance Hospital, Yonsei University College of Medicine, Seoul, Korea

Received: Nov 10, 2025
Revised: Jan 5, 2026
Accepted: Jan 15, 2026
Published online: Mar 16, 2026

Correspondence to
Sun Young Rha
Song-Dang Institute for Cancer Research, Division of Medical Oncology, Department of Internal Medicine, Yonsei Cancer Center, Yonsei University College of Medicine, 50-1 Yonsei-ro, Seodaemun-gu, Seoul 03722, Korea.
Email: rha7655@yuhs.ac

ORCID iDs
Ye Jin Moon
https://orcid.org/0009-0003-4293-3722
Woo Sun Kwon
https://orcid.org/0000-0003-0268-5624
Chan Hee Park
https://orcid.org/0000-0002-3820-686X
Jinsoo Jang
https://orcid.org/0009-0004-2573-1253
Juin Park
https://orcid.org/0000-0002-5006-1464
Byeong Gyu Yoon
https://orcid.org/0009-0007-0443-135X
Han Byeol Mun
https://orcid.org/0009-0000-2667-4562

ABSTRACT

Purpose: Patient-derived cells (PDCs) and patient-derived organoids (PDOs) are complementary preclinical models widely used in translational cancer research. However, their molecular and functional differences have not been systematically characterized. This study established and analyzed paired PDC and PDO models derived from the same gastric cancer ascites to delineate platform-dependent molecular and functional profiles.
Materials and Methods: Malignant ascites or pleural fluid obtained from 6 patients with advanced gastric cancer were used to establish paired PDC and PDO models. All pairs underwent comprehensive multi-omics profiling, integrating genomic, transcriptomic, and proteomic data. Phenotypic characterization included morphological, histological, proliferative, and cell cycle analyses. Drug sensitivity assays were performed using 4 chemotherapeutic agents commonly used to treat gastric cancer.
Results: The 6 paired PDC and PDO models exhibited distinct morphological characteristics. Whole-genome analyses demonstrated high concordance among primary tumors, PDCs, and PDOs, confirming tumor representation across platforms. Multi-omics profiling identified platform-dependent molecular signatures; PDOs were enriched for extracellular matrix remodeling and stemness, whereas PDCs displayed proliferation- and immune-related signatures. Clinically relevant biomarkers, including HER2 and MET alterations, were concordant with primary tumors. Notably, drug responses differed between platforms and patients, indicating platform-dependent and patient-specific chemosensitivity.
Conclusions: Paired PDC and PDO models derived from the same patients preserved core patient-specific tumor characteristics while exhibiting distinct molecular and functional profiles. These findings underscore the culture platform as a critical determinant of experimental outcomes and therapeutic responses. Therefore, careful selection of an appropriate preclinical model is essential to accurately address biological questions and optimize precision oncology strategies.

Keywords: Gastric cancer; Cell line, tumor; Organoids; Ascites; Multi-omics

jgc Journal of Gastric Cancer

Namju Kim
https://orcid.org/0009-0006-5028-3549
Choong-kun Lee
https://orcid.org/0000-0001-5151-5096
Hei Cheul Jeung
https://orcid.org/0000-0003-0952-3679
Su-Jin Shin
https://orcid.org/0000-0001-9114-8438
Tae Soo Kim
https://orcid.org/0009-0006-7996-3409
Sun Young Rha
https://orcid.org/0000-0002-2512-4531

Presentation
This manuscript was presented at the American Association for Cancer Research (AACR)– Korean Cancer Association (KCA) Joint Conference 2024 (Fall), Seoul, Korea; the AACR Annual Meeting 2025, Chicago, IL, USA; and the KCA–Asian Oncology Society (AOS) Joint Meeting 2025 (Spring), Seoul, Korea.

Funding
This study was supported by the National Research Foundation of Korea (NRF) grant funded by the Korean government (MSIT) (2020R1A2B5B02001452).

Conflict of Interest
No potential conflict of interest relevant to this article was reported.

Author Contributions
Conceptualization: M.Y.J., K.W.S., J.H.C., L.C.K., R.S.Y.; Data curation: M.Y.J., K.W.S., K.T.S., S.S.J., J.J., P.J., Y.B.G., M.H.B.; Formal analysis: M.Y.J., P.C.H., K.N.; Investigation: M.Y.J., K.W.S.; Writing - original draft: M.Y.J., K.W.S., P.C.H., R.S.Y.

INTRODUCTION

Preclinical models are essential for understanding cancer biology and developing effective therapies. Although 2-dimensional (2D) cultures are widely used, they often fail to simulate the complex tumor microenvironment (TME) [1-3]. Nevertheless, conventional 2D cultures offer practical advantages for preclinical research, as they are technically straightforward, proliferate rapidly, and readily adaptable to high-throughput screening and genetic manipulation. However, 2D cultures impose a selective pressure that preferentially expands rapidly proliferating clones, reducing cellular heterogeneity compared with the primary tumors. This selection can lead to transcriptomic and phenotypic divergence from the original tumor and limit the fidelity in predicting patient-specific therapeutic responses [4].

In contrast, 3-dimensional (3D) cultures preserve tumor heterogeneity and architecture, providing more physiologically relevant insights into tumor biology and treatment responses [5-7]. Several studies, particularly those on gastrointestinal cancers, have reported that 3D models can predict clinical responses [8] and better capture cell–cell and matrix interactions. However, 3D platforms are more resource-intensive, have limited scalability, and typically lack the stromal and immune components of the native TME. Moreover, most 3D models have been established from primary tumors, with comparatively few derived from metastatic lesions, especially the ascitic fluid of metastatic gastric cancer [9]. This gap is notable because gastric cancer remains a leading cause of cancer mortality, and metastatic disease presents the greatest clinical challenge [10,11]. Recent studies have suggested that 3D models do not consistently outperform 2D models in predicting patient-specific drug responses [12,13]. Such discrepancies likely reflect intrinsic tumor heterogeneity and the influence of distinct culture environments on molecular and functional phenotypes [14-16].

Patient-derived cells (PDCs) and patient-derived organoids (PDOs) are valuable preclinical platforms. PDCs are scalable and experimentally tractable, whereas PDOs better preserve tumor architecture. However, few studies have directly compared the paired PDC and PDO models established from the same patient, particularly those for malignant ascites. Consequently, the fundamental differences in culture systems that shape molecular characteristics and drug sensitivity remain incompletely understood.

In this study, we established and characterized paired PDC and PDO models derived from the malignant ascites of patients with advanced gastric cancer. Through integrated multi-omics and functional analyses, we systematically compared their biological and molecular profiles to define platform-specific features and propose model-appropriate applications, thereby providing evidence-based guidance for model selection in translational research and precision oncology.

MATERIALS AND METHODS

Establishment of PDCs and PDOs

Following protocols from the Song-Dang Institute for Cancer Research (SICR), we established paired PDC and PDO models using malignant ascites or pleural effusion specimens from 6 patients with advanced gastric cancer [17]. All procedures were approved by the Institutional Review Board (IRB) of Severance Hospital, Yonsei University Health System (IRB No. 4-2014-0638), and written informed consent was obtained from all patients. Ascitic fluid

https://doi.org/10.5230/jgc.2026.26.e19

jgc Journal of Gastric Cancer

samples were assessed using hematoxylin and eosin staining to confirm the presence of tumor cells and estimate tumor purity prior to model establishment. Fluids were transferred to 50-mL tubes, washed with phosphate-buffered saline (PBS), and centrifuged to obtain cell pellets. For PDC culture, cell pellets were resuspended in minimum essential medium with Earle's salts and L-glutamine (Serana, Heidelberg, Germany) supplemented with 10% fetal bovine serum (Corning, Corning, NY, USA) and 1% penicillin–streptomycin (Gibco, Thermo Fisher Scientific, Waltham, MA, USA), and seeded into 25-cm^2 flasks. For PDO culture, pellets were resuspended in Cultrex Basement Membrane Extract Type 2 (BME; R&D Systems, Minneapolis, MN, USA), plated at 10 domes per well in 6-well plates, polymerized at 37 °C for 20 minutes, and overlaid with organoid medium. The medium was refreshed every 3–4 days and passaging was performed every 6–7 days, as previously described [17,18]. Cultures were maintained at 37°C in a humidified 5% CO_2 incubator. Stable models were defined at passage 5, and all downstream assays were conducted between passages 5 and 10. Short tandem repeat profiling at passage 5 verified the identity of paired PDCs, PDOs, and matched peripheral blood mononuclear cells (**Supplementary Table 1**).

Morphological and histological analyses

The morphologies of the established PDCs and PDOs were monitored between days 3 and 5 using a phase-contrast microscope and a high-content imaging system (Operetta CLS; PerkinElmer, Waltham, MA, USA). For histological analysis, cell blocks were prepared from the original fluids, PDCs, and PDOs. Fluids and PDCs were processed as formalin-fixed paraffin-embedded (FFPE) cell blocks using standard protocols, whereas PDO domes were fixed with 4% paraformaldehyde, washed with PBS, embedded in 3% ultra-low-gelling temperature agarose, and subsequently processed in paraffin. For immunohistochemical analysis, 3–4 μm sections were cut from FFPE cell blocks, deparaffinized, rehydrated, and subjected to heat-induced epitope retrieval based on standard procedures. Subsequently, sections were stained using the following primary reagents: anti-HER2/neu (4B5), anti-total c-MET (SP44), CLDN18 (43-14A) assay, INFORM EBER probe, anti-EGFR (SP84), anti-FGFR2b (FPR2-D), anti-PD-L1 (SP263), and anti-TP53 (DO-7), followed by chromogenic detection and hematoxylin counterstaining.

Genomic profiling

To evaluate how each model recapitulated the tumor of the patient, we compared somatic genetic alterations across matched primary tumors, PDCs, and PDOs in the 6 patients. Primary tumors were analyzed using in-house targeted deep sequencing with a CancerMaster panel (SICR, Yonsei University College of Medicine, Seoul, Korea; gene list in **Supplementary Table 2**). PDCs and PDOs underwent whole-genome sequencing (WGS) performed by INOCRAS (Daejeon, Korea). Sequencing reads were quality checked and mapped to the human reference genome (GRCh38), and somatic variants (SNVs/indels) were identified and annotated using a standardized pipeline. Variant calls from WGS of the PDC and PDO models were compared with panel-based calls from matched primary tumors to quantify molecular concordance and distinguish shared from model-specific alterations. The biological relevance of the mutations was assessed using the cBioPortal for Cancer Genomics.

Transcriptomic and proteomic profiling

To characterize platform-dependent biology, RNA sequencing (RNA-seq; INOCRAS) and LC–MS/MS proteomic analyses (National Cancer Center, Goyang, Korea) were performed. RNA-seq counts were normalized to transcripts per million (TPM) and log2-transformed, and protein intensities were similarly normalized and log2-transformed. Genes with TPM <50

https://doi.org/10.5230/jgc.2026.26.e19

jgc Journal of Gastric Cancer

across all samples and proteins not detected in any sample were excluded from downstream analyses. Global expression differences were visualized using unsupervised hierarchical clustering based on Euclidean distance with complete linkage. Differential expression analyses were performed using DESeq2 (Bioconductor, R v1.40.0); significance thresholds were set at false discovery rate (FDR)=0.05 with ≥4-fold change for RNA-seq, and FDR=0.10 with ≥2-fold change for proteomics. Gene Set Enrichment Analysis (GSEA) was conducted using GSEA v4.3.2 (Broad Institute, Cambridge, MA, USA) with MSigDB hallmark gene sets to identify pathways distinguishing PDCs from PDOs. Single-sample GSEA (ssGSEA) was performed to compute epithelial–mesenchymal transition (EMT) scores using the HALLMARK_EPITHELIAL_MESENCHYMAL_TRANSITION gene set.

Cell proliferation assay

Cell proliferation was measured using the Quanti-Max™ WST-8 Cell Viability Assay Kit (Biomax, Seoul, Korea). PDCs were seeded at a density of 5×10^3 cells/well in 96-well plates, whereas PDOs were seeded as 1×10^3 cells in a 4-μL dome of BME per well. Cell viability was monitored daily for 8 days by measuring absorbance at 450 nm using a microplate reader (800TS; BioTek Instruments, Winooski, VT, USA).

Cell cycle analysis

PDCs and PDOs were harvested at 24 and 72 hours after seeding, respectively. For drug-treatment, both models were treated for 72 hours with SN-38 (6.94 nM; Sigma-Aldrich, St. Louis, MO, USA), 5-fluorouracil (5-FU; 16.2 μM; Merck, Darmstadt, Germany), or oxaliplatin (8.33 μM; Sigma-Aldrich) at concentrations based on reported C_{max} values [19]. Cells were fixed in 70% ethanol at −20°C overnight, washed with PBS, and stained with propidium iodide/RNase staining buffer (BD Pharmingen™, San Diego, CA, USA). Data were acquired using a BD Accuri™ C6 Plus flow cytometer (BD Biosciences, San Jose, CA, USA) and analyzed using FlowJo version 10.7.1 (BD Biosciences) [20].

Flow cytometry

To quantify cell surface HER2, 5×10^5 cells from both PDCs and PDOs were stained for 15 minutes at 4°C in the dark with either APC-conjugated anti-human CD340 (erbB2/HER2) antibody (1:30 dilution; BioLegend, San Diego, CA, USA) or APC-conjugated mouse IgG1 κ isotype control antibody (1:30 dilution; BioLegend). Breast cancer cell lines SK-BR-3 (3+), ZR-75-1 (2+), and HCC-1937 (0) were used as controls [21]. Subsequently, cells were washed with cell staining buffer (BioLegend). Flow cytometry was performed using an Accuri™ C6 Plus flow cytometer (BD Biosciences). Data were analyzed using FlowJo version 10.7.1 (BD Biosciences).

Immunoblotting

Whole-cell protein lysates from PDCs and PDOs were prepared as previously described, and 20–30 μg per sample was used for sodium dodecyl sulfate polyacrylamide gel electrophoresis and immunoblotting [22]. Membranes were incubated overnight at 4°C with primary antibodies against MET (1:1,000; Santa Cruz Biotechnology, Dallas, TX, USA) and glyceraldehyde 3-phosphate dehydrogenase (GAPDH) (1:5,000; Abcam, Cambridge, UK), with GAPDH serving as the loading control. After washing, membranes were incubated with horseradish peroxidase–conjugated secondary antibodies (1:5,000) for 1 hour at 25°C. Signals were detected using a ChemiDoc™ XRS+ imaging system (Bio-Rad, Hercules, CA, USA) and quantified using Image Lab v6.0 (Bio-Rad). Lysates from YCC-31 and SNU-5 cells served as positive controls, whereas AGS lysate was used as a negative control.

https://doi.org/10.5230/jgc.2026.26.e19

jgc Journal of Gastric Cancer

Drug sensitivity

Drug sensitivity was assessed using 4 chemotherapeutic agents: paclitaxel (Sigma-Aldrich), SN-38, 5-FU, and oxaliplatin. PDCs were seeded at 5×10^4 cells/well, and PODs at 1×10^3 cells/well in 4 μL BME, in 96-well plates. After stabilization for 24 hours (PDCs) or 72 hours (PDOs), the models were treated with variable drug concentrations for 72 hours. Cell viability was evaluated using the Quanti-Max™ WST-8 Cell Viability Assay Kit (Biomax), with absorbance measured at 450 nm using a microplate reader (800TS; BioTek Instruments) [23]. All experiments were performed in triplicates and repeated independently at least twice. Dose–response curves were generated, and half-maximal inhibitory concentrations (IC_{50}) were calculated using CalcuSyn v2.11 (Biosoft, Cambridge, UK).

Statistical analysis

All experiments included at least 3 biological replicates. Quantitative data are presented as mean ± standard deviation, unless otherwise specified. For assays with only 2 biological replicates per condition (n=2), including cell proliferation, cell cycle, and drug sensitivity, no statistical significance testing was performed owing to the limited sample size.

RESULTS

Morphological and histological features of PDCs and PDOs

Paired patient-derived models were established from malignant ascites or pleural fluid samples obtained from 6 patients with advanced gastric cancer, each presenting distinct morphological and histological characteristics (**Table 1**). All specimens had tumor purity >30%, were proficient mismatch repair/microsatellite stable, and were negative for the Epstein–Barr virus (EBV). Histological evaluation of the original fluids revealed cytomorphological diversity across cases (**Fig. 1**). Specifically, YCC-GO10-1 and YCC-GO58-2 exhibited dispersed tumor cells with nuclear pleomorphism, whereas YCC-GO30 and YCC-GO6 formed cohesive epithelial clusters with relatively uniform nuclei and abundant cytoplasm. YCC-GO9 and YCC-GO60 showed intermediate features, with mixed patterns of single cells and small clusters. The PDC models displayed 2 distinct growth patterns: adherent and semi-suspended. YCC-GO10-1, YCC-GO30, and YCC-GO9 formed adherent monolayers characterized by flattened polygonal cells with well-defined borders and polarities under phase-contrast microscopy, whereas YCC-GO58-2, YCC-GO60, and YCC-GO6 grew in semi-suspensions, as loosely attached clusters with greater morphological heterogeneity. Nonetheless, all PDCs retained their epithelial characteristics under 2D conditions. In contrast, PDOs cultured in 3D culture exhibited 2 distinct growth

Table 1. Clinical characteristics of patients with gastric cancer used for model establishment

Patient characteristics	YCC-GO10-1	YCC-GO30	YCC-GO9	YCC-GO58-2	YCC-GO60	YCC-GO6
Age (yr)	38	60	52	40	72	34
Sex	Female	Female	Female	Male	Female	Male
Lauren classification	Intestinal	Unknown	Diffuse	Unknown	Unknown	Unknown
Histology	APD	SRC/PCC	AMD	AMD+SRC/PCC	SRC/PCC	SRC/PCC
HER2 (IHC)	High (3+)	None	Low (1+)	None	None	Low (1+)
MET (TSO500)	Amplification	None	None	Amplification	None	Amplification
Origin	Peritoneal fluid	Peritoneal fluid	Peritoneal fluid	Pleural fluid	Peritoneal fluid	Peritoneal fluid
Tumor purity (in fluid; %)	50	90	90	60	30	80
Survival from fluid collection (mo)	4.4	5.5	1.5	0.6	0.4	2.5

APD = adenocarcinoma, poorly differentiated; SRC/PCC = signet ring cell carcinoma/poorly cohesive carcinoma; AMD = adenocarcinoma, moderately differentiated; AMD+SRC/PCC = moderately differentiated adenocarcinoma with signet ring cell components in the background of low-grade epithelial dysplasia; IHC = immunohistochemistry.

https://doi.org/10.5230/jgc.2026.26.e19

jgc Journal of Gastric Cancer

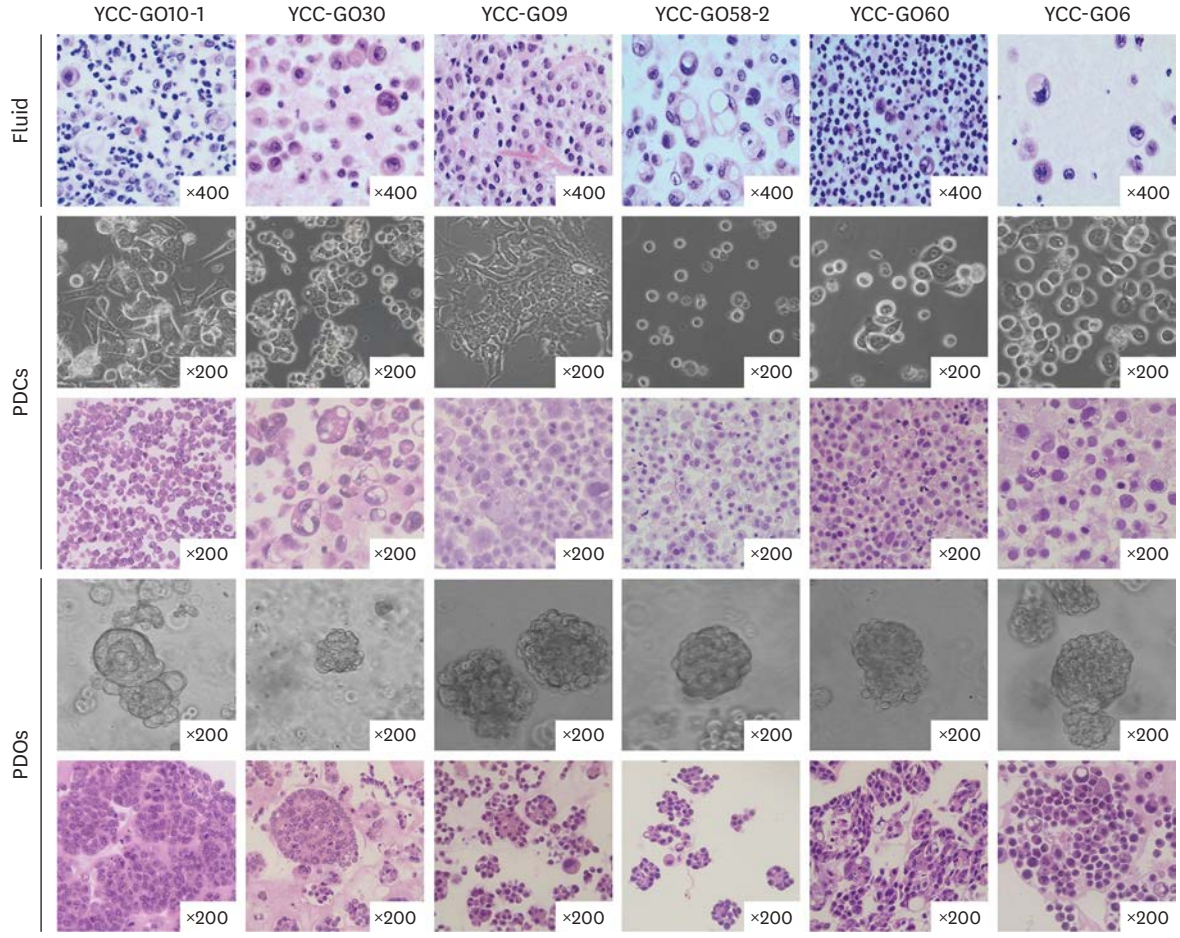

Fig. 1. Morphological characteristics of patient-derived models. Representative images comparing the original malignant ascitic or pleural fluid (top row) with the subsequently established patient-derived models. Hematoxylin and eosin staining of the fluid shows dispersed tumor cells. Bright-field images of PDCs reveal 2 growth patterns: adherent (YCC-GO10-1, YCC-GO30, YCC-GO9) and semi-suspension (YCC-GO58-2, YCC-GO60, YCC-GO6). PDOs form 3-dimensional structures with varying morphologies, including compact (YCC-GO10-1, YCC-GO58-2, YCC-GO60) and grape-like (YCC-GO30, YCC-GO9, YCC-GO6) clusters. Magnifications are indicated on the images.
PDC = patient-derived cell; PDO = patient-derived organoid.

morphotypes. YCC-GO10-1, YCC-GO58-2, and YCC-GO60 predominantly formed compact organoids, whereas YCC-GO30, YCC-GO9, and YCC-GO6 formed grape-like structures with loosely aggregated clusters. Histological analysis revealed multilayered, cystic, and rounded epithelial structures in PDOs, indicating greater spatial organization than that of their matched PDCs.

Genomic fidelity and model-dependent multi-omics profiling

Genomic profiling of primary tumors and matched PDC and PDO models showed overall concordance in major driver alterations across culture platforms, while revealing model-restricted variants in several genes (**Fig. 2A**). Among the 6 patient pairs, matched primary tumor, PDC, and PDO sets were available for 4 cases. In YCC-GO9, WGS was performed for the primary tumor and PDCs only, as the corresponding PDOs repeatedly failed quality control during culture and library preparation. In YCC-GO60, only PDCs and PDOs were sequenced owing to insufficient primary tumor material. These discrepancies likely reflect a combination of ascites-derived metastatic or peritoneal-seeding subclones, spatial and temporal intra-tumoral heterogeneity between the sampled primary tissue and

https://doi.org/10.5230/jgc.2026.26.e19

fluid-derived cells, and clonal selection or enrichment during ex vivo culture. In contrast to genomic concordance, transcriptomic and proteomic profiling revealed platform-dependent divergence. Transcriptomic principal component analysis (PCA) and unsupervised hierarchical clustering separated PDCs from PDOs, whereas proteomic profiles were clustered predominantly by paired samples, with some model-specific grouping evident in PCA (**Supplementary Fig. 1A and B**). Consistently, hierarchical clustering using all detected transcripts and proteins showed a pronounced model-based separation at the transcriptomic level, whereas proteomic profiles remained largely organized by patient pairing (**Supplementary Fig. 1C and D**). This pattern reinforces that protein expression retains stronger patient-of-origin constraints than the more divergent transcriptomic profiles. Differential expression analysis identified 5,534 differentially expressed genes (DEGs) from RNA-seq and 11,963 differentially expressed proteins (DEPs) from proteomics, with hierarchical clustering showing clear model-based grouping (**Fig. 2B and C**). Notably, these DEG- and DEP-based heatmaps highlight distinct sets of model discriminatory features rather than global abundance patterns, which can otherwise suggest a platform-wide shift in signal intensity. Transcript and protein levels are only partially coupled because of post-transcriptional regulation and protein turnover, and the 3D organoid context is expected

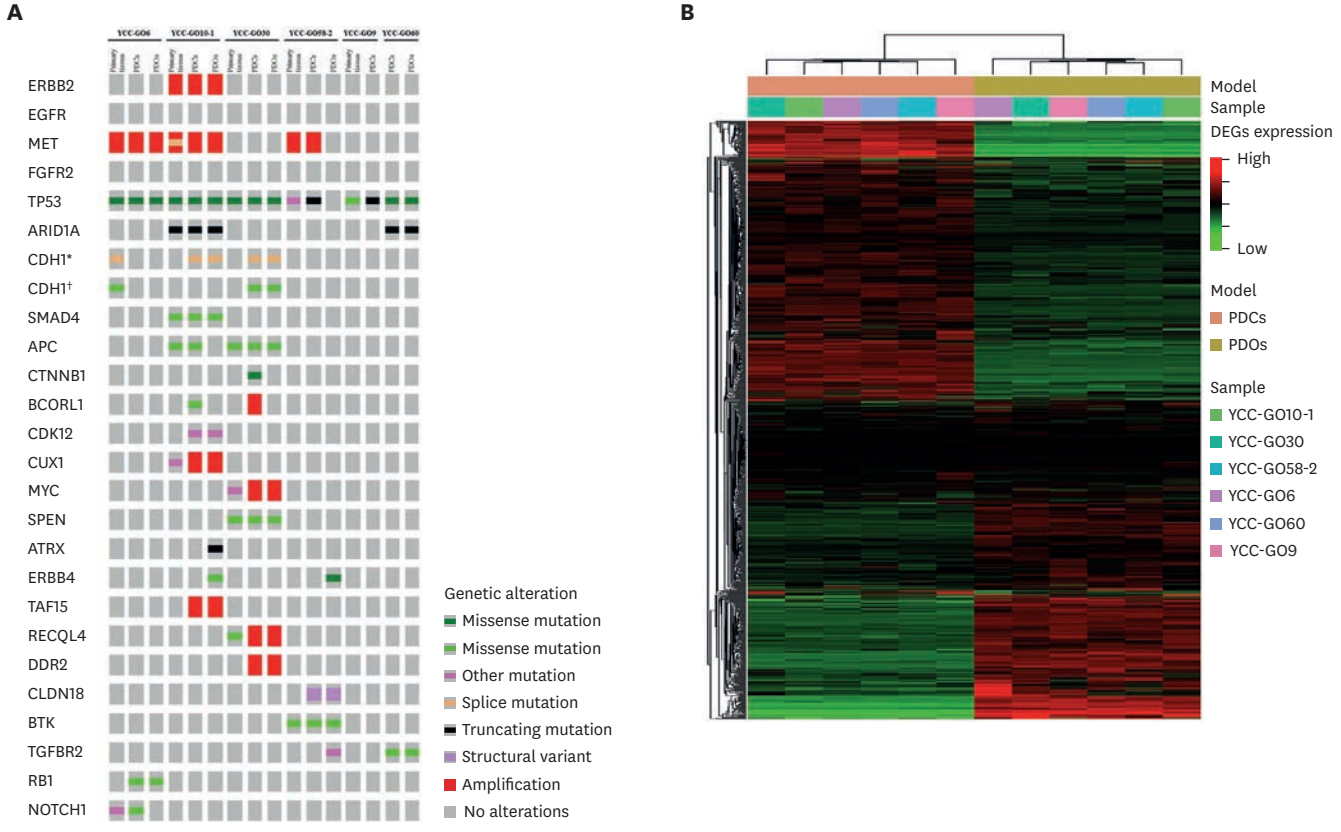

Fig. 2. Genomic and multi-omics profiling of patient-derived models. (A) Oncoprint depicting somatic alterations in primary tissues and their paired patient-derived models. The alteration patterns demonstrate strong concordance between tissues and their matched models, with notable model-specific differences in mutational profiles. (B, C) DEGs and DEPs were identified through differential analysis and subjected to hierarchical clustering. The clustering shows distinct separation of samples by model type (PDCs vs. PDOs), indicating model-specific gene and protein expression profiles. (D, E) GSVA scores derived from DEGs and DEPs highlight platform-dependent pathway activity. DEG-derived GSVA scores are generally higher in PDCs, whereas DEP-derived scores are more pronounced in PDOs, suggesting distinct biological activity in each model type.
DEG = differentially expressed gene; DEP = differentially expressed protein; PDC = patient-derived cell; PDO = patient-derived organoid; GSVA = Gene Set Variation Analysis.
*c.1320+1G>T; †G239R.

(continued to the next page)

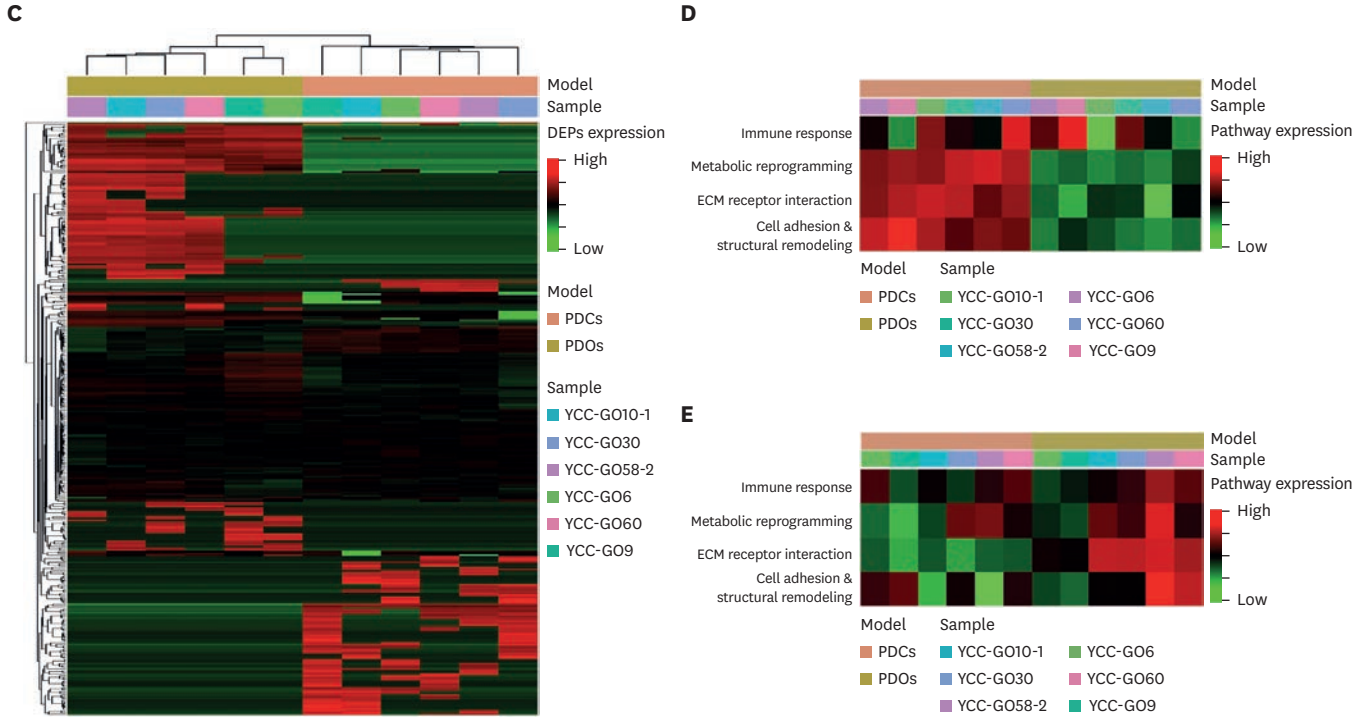

Fig. 2. (Continued) Genomic and multi-omics profiling of patient-derived models. (A) Oncoprint depicting somatic alterations in primary tissues and their paired patient-derived models. The alteration patterns demonstrate strong concordance between tissues and their matched models, with notable model-specific differences in mutational profiles. (B, C) DEGs and DEPs were identified through differential analysis and subjected to hierarchical clustering. The clustering shows distinct separation of samples by model type (PDCs vs. PDOs), indicating model-specific gene and protein expression profiles. (D, E) GSVA scores derived from DEGs and DEPs highlight platform-dependent pathway activity. DEG-derived GSVA scores are generally higher in PDCs, whereas DEP-derived scores are more pronounced in PDOs, suggesting distinct biological activity in each model type.
DEG = differentially expressed gene; DEP = differentially expressed protein; PDC = patient-derived cell; PDO = patient-derived organoid; GSVA = Gene Set Variation Analysis.
*c.1320+1G>T; †G239R.

to preferentially stabilize extracellular matrix (ECM) adhesion and structural proteins. Collectively, these factors likely explain why PDC-enriched patterns are more prominent at the transcript level, whereas PDO-enriched patterns are more evident at the protein level. Pathway enrichment analysis indicated complementary biology across the omics layers (**Fig. 2D and E**). In the transcriptome, PDCs were enriched in metabolic and immune response pathways, whereas PDOs were enriched in stress response, DNA repair, and metabolic reprogramming pathways. In the proteome, PDCs exhibited a cytoskeletal/metabolic baseline without prominent ECM remodeling, whereas PDOs were enriched for ECM–receptor interactions and structural remodeling signatures, accompanied by relative depletion of ferroptosis and secretory pathways. Collectively, these data indicate that, although genomic alterations are preserved across platforms, transcriptomic and proteomic profiles are shaped by the culture environment, producing a platform-dependent biological phenotype.

EMT profiling to understand metastatic potential

DEG-based enrichment aligned with PDC-associated pathways, whereas DEP-based enrichment aligned with PDO-associated ECM and structural remodeling pathways, resulting in model-driven segregation. To further explore the biological basis of this divergence, we focused on EMT, a process intimately associated with ECM remodeling, invasion, and metastatic plasticity. In proteomics, unsupervised hierarchical clustering using the MSigDB Hallmark EMT gene set segregated samples by culture model (PDOs vs. PDCs) rather

https://doi.org/10.5230/jgc.2026.26.e19

jgc Journal of Gastric Cancer

than patient identity, with consistently higher EMT-related protein abundance observed in PDOs (**Fig. 3A**). Similarly, ssGSEA-derived EMT scores were significantly higher in PDOs than in matched PDCs across all pairs (**Fig. 3B**). Epithelial markers, such as EPCAM and CDH1, were maintained on both platforms, whereas mesenchymal markers involved in ECM remodeling and migration, including ITGB3 and LOXL2, were markedly upregulated in PDOs. To functionally validate these proteomics-based EMT signatures, western blot analysis demonstrated E-cadherin expression in all samples, with higher levels in PDOs than in the corresponding PDCs, whereas Vimentin was not appreciably expressed in either model (**Fig. 3C and D**). These findings indicate that elevated EMT/ECM signatures in PDOs primarily reflect culture context–dependent remodeling and epithelial–mesenchymal plasticity rather than full mesenchymal conversion, and that enhanced E-cadherin expression is consistent with strengthened junctional/adhesion features in the 3D organoid architecture. However,

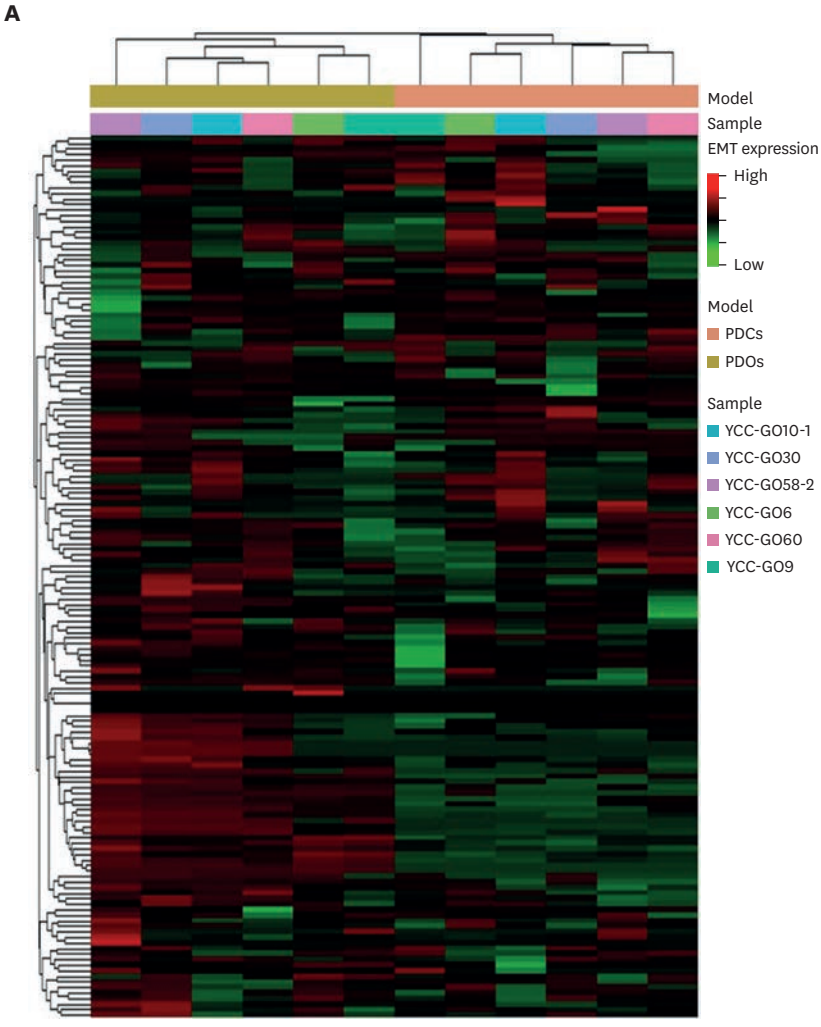

Fig. 3. Proteomic EMT signatures in PDCs and PDOs. (A) Unsupervised hierarchical clustering of all samples using the MSigDB Hallmark EMT protein set demonstrates segregation primarily by culture model (PDCs vs. PDOs), with higher EMT-related protein abundance in PDOs than in paired PDCs. (B) Single-sample Gene Set Enrichment Analysis-derived EMT scores showing consistently higher EMT activity in PDOs than in matched PDCs across all 6 pairs. (C, D) Immunoblot analysis of EMT markers in representative paired models, assessing E-cadherin and Vimentin expression. Gastric cancer cell lines (YCC-25, AGS, and SNU-484) were included as controls; α-tubulin and GAPDH served as loading controls. In both patient pairs, E-cadherin was detectable in PDCs and further increased in PDOs, whereas Vimentin was minimal or absent, consistent with an epithelial phenotype with limited mesenchymal transition.
EMT = epithelial–mesenchymal transition; PDC = patient-derived cell; PDO = patient-derived organoid; GAPDH = glyceraldehyde 3-phosphate dehydrogenase.

(continued to the next page)

https://doi.org/10.5230/jgc.2026.26.e19

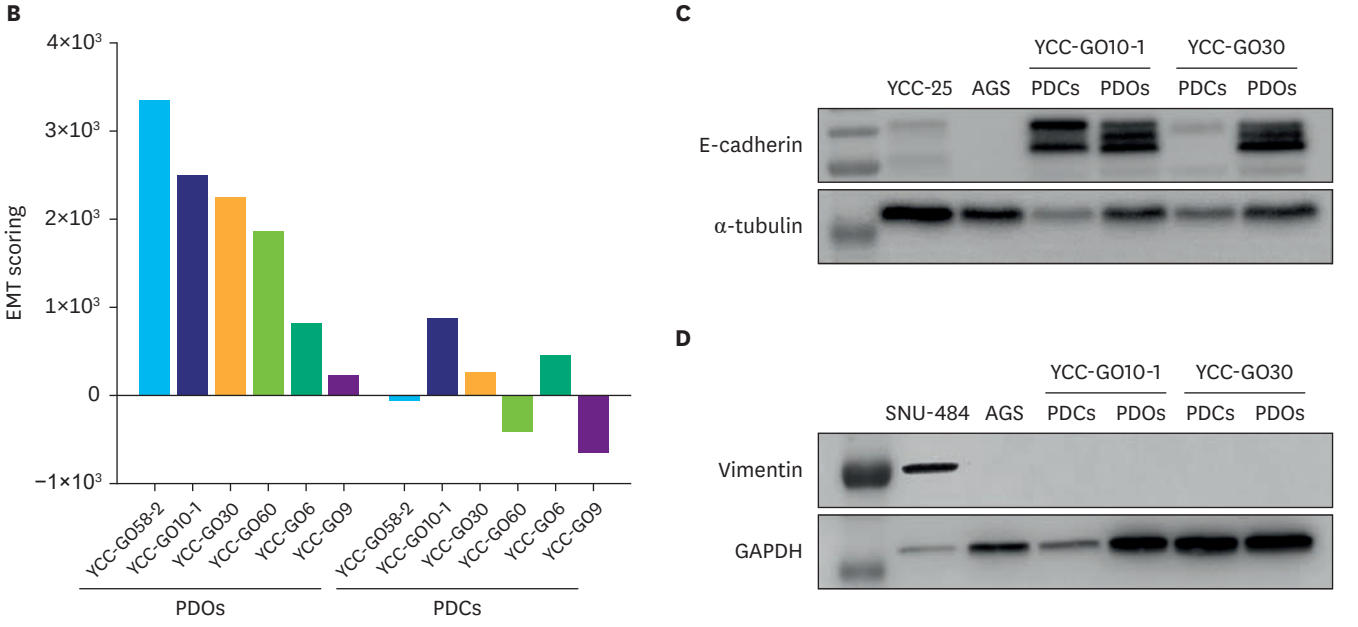

Fig. 3. (Continued) Proteomic EMT signatures in PDCs and PDOs. (A) Unsupervised hierarchical clustering of all samples using the MSigDB Hallmark EMT protein set demonstrates segregation primarily by culture model (PDCs vs. PDOs), with higher EMT-related protein abundance in PDOs than in paired PDCs. (B) Single-sample Gene Set Enrichment Analysis-derived EMT scores showing consistently higher EMT activity in PDOs than in matched PDCs across all 6 pairs. (C, D) Immunoblot analysis of EMT markers in representative paired models, assessing E-cadherin and Vimentin expression. Gastric cancer cell lines (YCC-25, AGS, and SNU-484) were included as controls; α-tubulin and GAPDH served as loading controls. In both patient pairs, E-cadherin was detectable in PDCs and further increased in PDOs, whereas Vimentin was minimal or absent, consistent with an epithelial phenotype with limited mesenchymal transition.
EMT = epithelial–mesenchymal transition; PDC = patient-derived cell; PDO = patient-derived organoid; GAPDH = glyceraldehyde 3-phosphate dehydrogenase.

application of the same Hallmark EMT gene set to RNA-seq data produced clustering predominantly by patient identity, with broadly comparable EMT scores between PDCs and PDOs, indicating limited model separation at the transcriptomic level (**Supplementary Fig. 2**). Collectively, these findings indicate that EMT and ECM-remodeling programs associated with metastatic plasticity are more distinctly captured at the protein level and are preferentially enriched in PDOs relative to their paired PDCs.

Basal proliferation and cell-cycle features of paired models

Among the 6 paired models, YCC-GO10-1 and YCC-GO30 were selected for functional assays based on their stable long-term growth under standardized conditions and representative paired phenotypes, including clinically relevant contrasts in drug-response concordance. To characterize basal cell-cycle regulation in these models, pathway activities related to cell-cycle arrest and phase transitions were quantified using Z-score–based scoring (**Fig. 4A and B**). Across both pairs, PDCs generally showed higher activity of core cell-cycle programs, including overall cell-cycle and phase-transition signatures. In YCC-GO10-1, model differences in these cell-cycle pathways were less pronounced, suggesting that the degree of pathway attenuation is patient-pair dependent rather than uniformly platform specific. In contrast, in YCC-GO30, PDOs exhibited coordinated reductions in cell-cycle progression pathways relative to paired PDCs, indicating a shift toward a slow-cycling baseline state in the 3D context. In both patient models, PDCs exhibited shorter doubling times than their matched PDOs (YCC-GO10-1: 43.2 vs. 69.7 hours; YCC-GO30: 56.1 vs. 77.9 hours), consistent with the higher cell cycle pathway activities observed in PDCs. Despite this difference in growth rate, overall growth patterns were comparable within each pair, with both models showing a gradual and consistent increase over the culture period

https://doi.org/10.5230/jgc.2026.26.e19

jgc Journal of Gastric Cancer

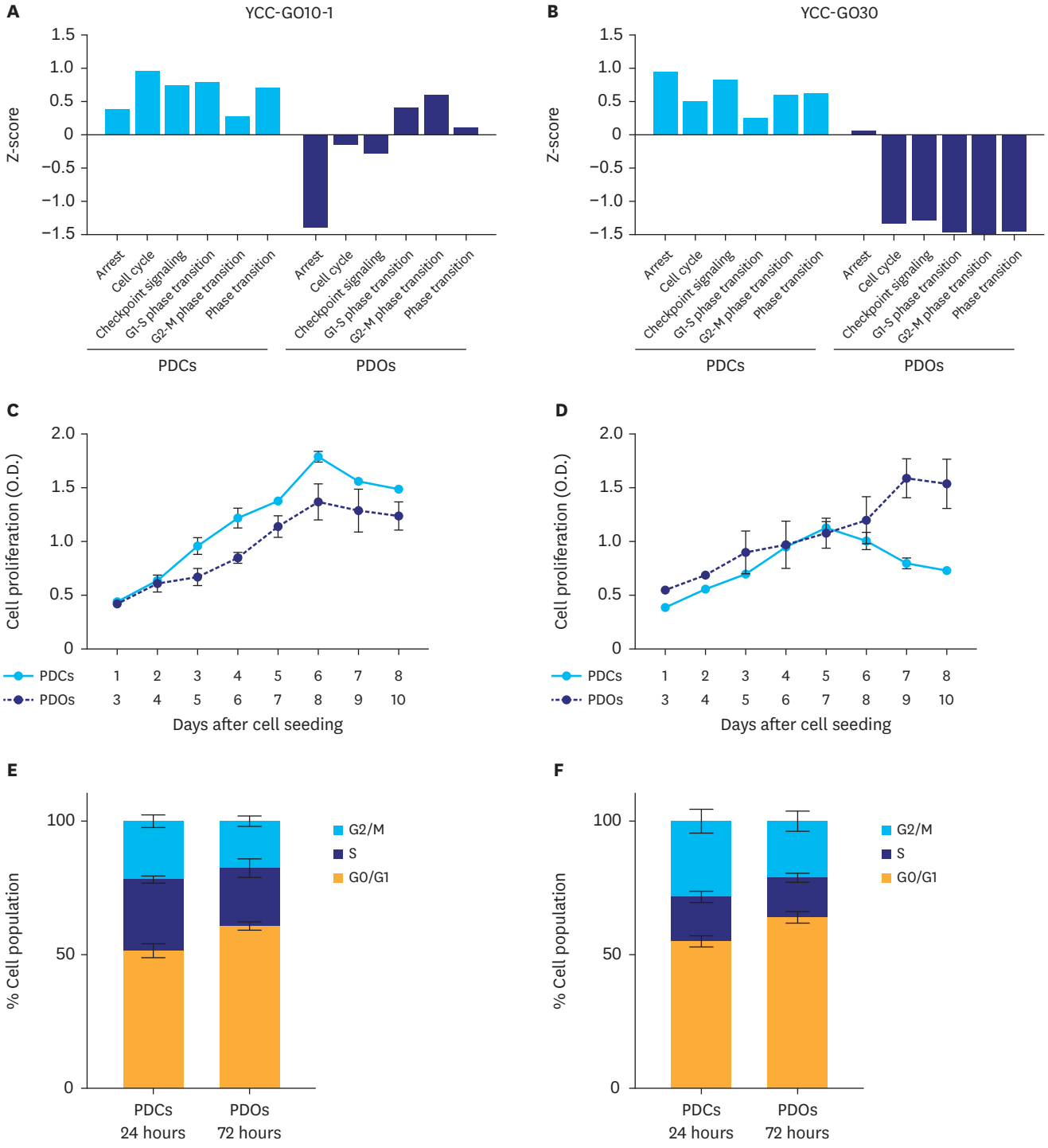

Fig. 4. Basal proliferation and cell cycle dynamics in paired models (n=2). (A, B) Z-score-based pathway activities for cell cycle regulation programs in YCC-GO10-1 (A) and YCC-GO30 (B), showing generally higher cell cycle activities in PDCs and a coordinated reduction in progression pathways in YCC-GO30 PDOs. (C, D) Proliferation curves for YCC-GO10-1 (C) and YCC-GO30 (D) measured daily over 8 days. PDCs show a higher initial proliferation rate, whereas PDOs exhibit more sustained growth over the extended culture period. (E, F) Cell cycle distribution for YCC-GO10-1 (E) and YCC-GO30 (F). Bar graphs display the percentage of cells in each phase (G0/G1, S, G2/M) at 24 hours for PDCs and 72 hours for PDOs. Both models predominantly reside in the G0/G1 phase with minimal sub-G1 populations, suggesting low apoptosis and active cell cycling. Data are presented as mean ± standard deviation.
PDC = patient-derived cell; PDO = patient-derived organoid; O.D. = optical density.

https://doi.org/10.5230/jgc.2026.26.e19

jgc Journal of Gastric Cancer

(**Fig. 4C and D**). Baseline cell cycle composition supported these proliferative trends: both platforms were predominantly composed of cells in the G0/G1 phase, with minimal sub-G1 fractions. However, PDOs consistently exhibited a higher G0/G1 and correspondingly lower S/G2–M fractions than their paired PDCs (**Fig. 4E and F**), indicating slower cell cycle progression in 3D culture conditions. Collectively, these pathway-level and functional data indicate that PDOs, particularly in YCC-GO30, adopt a slow cycling state characterized by attenuated cell cycle programs and G0/G1 accumulation, whereas PDCs retain more active cell-cycle signatures despite overall concordant growth trajectories within each patient pair.

HER2 and MET expression

HER2 (ERBB2) and MET levels were examined in the 2 representative pairs to determine how patient-specific receptor alterations are reflected at the protein level in each culture system (**Table 1**, **Supplementary Table 3**). ERBB2 copy-number status was concordant within pairs (YCC-GO10-1 amplified, ≈22 copies; YCC-GO30 non-amplified, <5 copies), and fluorescence-activated cell sorting analysis showed high HER2 expression in YCC-GO10-1 and uniformly low expression in YCC-GO30, consistent with the genomic findings (**Fig. 5A**). Within YCC-GO10-1, PDCs displayed higher mean fluorescence intensity than the matched PDOs; however, both models preserved the overall HER2-high phenotype. Notably, HER2 heterogeneity was more evident in the PDOs: PDCs showed a unimodal, uniformly high signal, whereas PDOs exhibited a bimodal distribution with distinct HER2-high and HER2-low subpopulations, indicating that subclonal variation in HER2 expression is more readily detected in the 3D model. MET profiling showed a similar genotype–protein relationship. WGS identified high-level MET amplification in YCC-GO10-1 (≈33–34 copies) but not in YCC-GO30 (<5 copies); immunoblotting confirmed strong MET expression in YCC-GO10-1 and weak or absent expression in YCC-GO30, without a consistent difference between 2D and 3D platforms (**Fig. 5B-D**). These results indicate that patient-specific HER2 and MET alterations are faithfully maintained at the protein level in both PDCs and PDOs, while HER2-amplified PDOs additionally reveal subclonal variability not apparent in bulk PDC measurements. To extend these observations across a broader panel, immunohistochemistry was performed for 8 clinically relevant markers (HER2, c-MET, CLDN18.2, EBV, EGFR, FGFR2, PD-L1, and TP53) across 6 paired PDC and PDO samples (YCC-GO10-1, YCC-GO30, YCC-GO9, YCC-GO58-2, YCC-GO60, and YCC-GO6) (**Supplementary Figs. 3** and **4**). Overall, staining patterns were largely concordant between matched 2D and 3D models within each patient, supporting the preservation of key receptor and lineage features across platforms. Nonetheless, occasional discrepancies in intensity or fraction of positive cells highlighted intra- and inter-model heterogeneity, which may influence targetable signaling and biomarker interpretation in individual cases.

Chemotherapeutic response and cell-cycle dynamics

To evaluate chemotherapeutic responses, paired PDC and PDO models were treated with paclitaxel, SN-38, 5-FU, and oxaliplatin, and dose response curves were generated (**Fig. 6A and B**). Drug sensitivity was strongly patient-dependent. In YCC-GO10-1, PDCs and PDOs exhibited concordant sensitivity, with nearly overlapping dose-response curves and comparable IC_{50} values across all 4 agents. In contrast, YCC-GO30 showed divergent responses based on culture model; although PDCs remained sensitive, PDOs were comparatively resistant to SN-38, 5-FU, and oxaliplatin. To assess clinical relevance, IC_{50} values were compared with the reported human C_{max}. In YCC-GO10-1, IC_{50} values for both models were below or near the C_{max} for all agents, consistent with predicted sensitivity. In YCC-GO30, PDC IC_{50} values were near the C_{max}, whereas PDO IC_{50} values for SN-38, 5-FU,

https://doi.org/10.5230/jgc.2026.26.e19

jgc Journal of Gastric Cancer

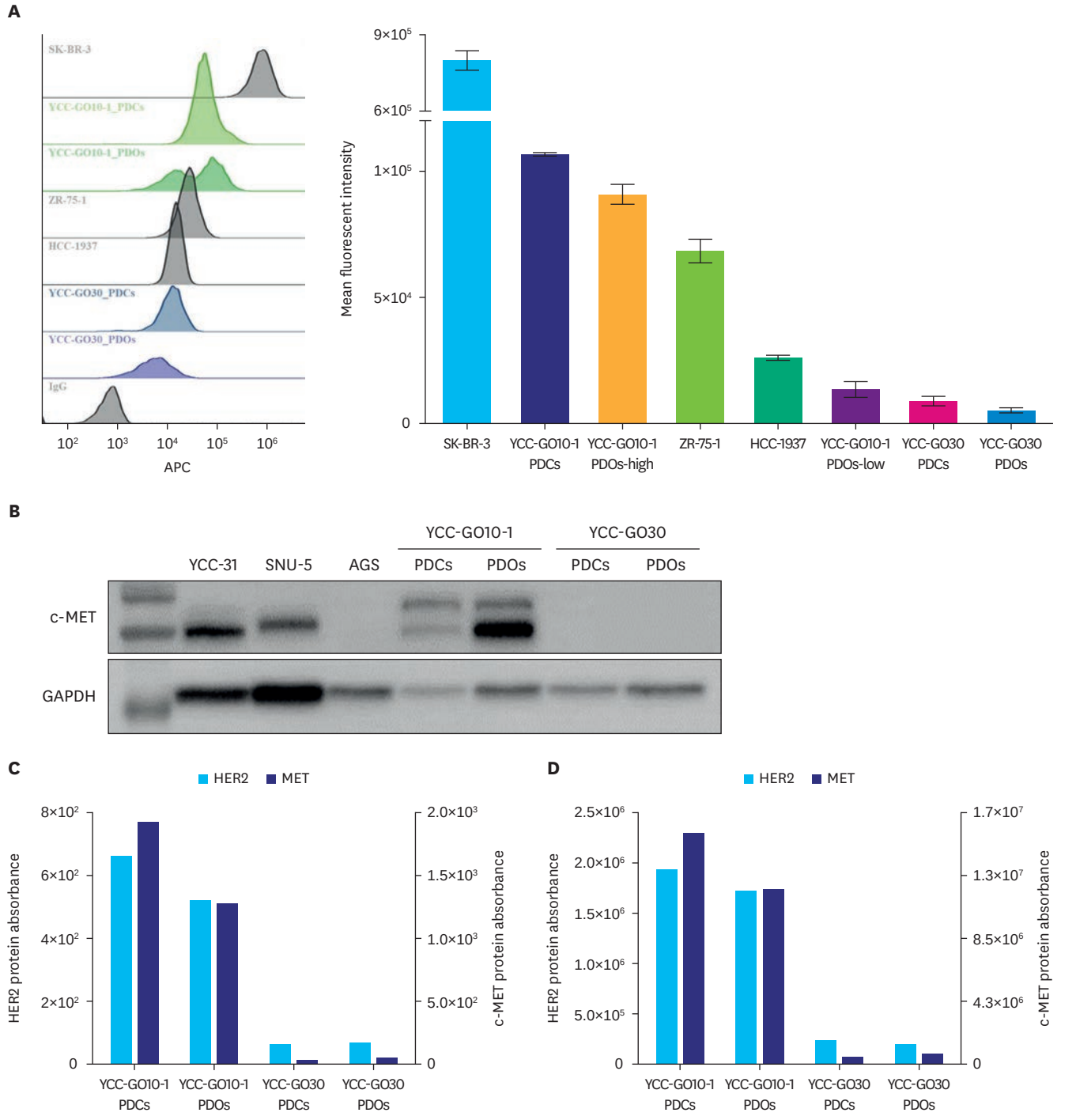

Fig. 5. HER2 and MET protein expression (n=2). (A) Flow cytometric quantification of HER2 surface expression, reported as MFI. The bar chart compares HER2 levels in paired PDCs and PDOs from YCC-GO10-1 and YCC-GO30 against a panel of control cell lines. The models recapitulated the HER2 immunohistochemical status of the original tumors (YCC-GO10-1: 3+; YCC-GO30: 0). Data are presented as mean ± standard deviation. (B) Immunoblot analysis showing MET protein expression confined to YCC-GO10-1 PDCs and PDOs. (C, D) Quantification of HER2 and MET expression from transcriptomic (C) and global quantitative proteomic (D) analyses, showing higher expression in YCC-GO10-1 than in YCC-GO30, consistent with amplification patterns observed in genomic profiling.
MFI = mean fluorescence intensity; PDC = patient-derived cell; PDO = patient-derived organoid.

https://doi.org/10.5230/jgc.2026.26.e19

jgc Journal of Gastric Cancer

and oxaliplatin exceeded the C_{max}, indicating PDO-specific resistance. Cell cycle analyses reflected the diversity in drug response patterns across the culture models (**Fig. 6C and D**). In the anti-cancer drug sensitivity of paired YCC-GO10-1 cells, each agent induced distinct phase redistributions: SN-38 increased S/G2–M fractions; 5-FU caused S-phase accumulation accompanied by an increase in the sub-G1 apoptotic fraction; and oxaliplatin led to G2/M enrichment. In contrast, in YCC-GO30—particularly in PDOs—the distribution remained largely unchanged relative to that in the control, consistent with functional drug resistance. To elucidate the mechanisms underlying these patient- and model-dependent drug response patterns, baseline proteomic profiles were examined. In the concordant pair YCC-GO10-1, pathway activities and key resistance markers were broadly comparable between PDCs and PDOs, consistent with near-overlapping dose–response curves and clear drug-induced changes in cell-cycle distribution. However, in YCC-GO30, PDOs showed marked enrichment of resistance-associated programs relative to paired PDCs, including xenobiotic metabolism, multiple stress-response, and microenvironmental pathways. This model-specific rewiring was further illustrated by comparative analysis of baseline protein abundance in curated drug-related markers between paired PDCs and PDOs (**Fig. 6E**). Although paclitaxel-associated markers showed minimal separation between the 2 models, distinct differences were observed for agents with functional divergence. For SN-38, YCC-GO30 PDOs displayed higher levels of the microenvironment- and TGF-β-modulating factor GREM2, whereas PDCs were enriched for transport and detoxification components, such as ATP1A4 and BCHE, consistent with a more directly drug-exposed, chemosensitive state. For 5-FU, PDOs showed upregulation of SHBG, in contrast to PDCs, which expressed higher levels of metabolism- and signaling-related factors such as SLC2A4 and DLG4 in PDCs, reflecting greater vulnerability of the more proliferative compartment to antimetabolite stress. For oxaliplatin, PDOs preferentially expressed stemness- and stress-adaptation markers, including PHF21B and MPO, whereas PDCs showed relatively higher levels of CST1 and SLC2A4, consistent with enhanced sensitivity of the latter to DNA-damaging insults. Collectively, these patterns indicate that the attenuated responses of YCC-GO30 PDOs to SN-38, 5-FU, and oxaliplatin reflect a broadly drug-tolerant baseline state rather than a single efflux- or target-level alteration.

DISCUSSION

Paired PDC and PDO models from gastric cancer ascites revealed fundamental, platform-dependent differences in tumor biology despite a shared genomic background [24]. In this study, we present the first direct and systematic comparison of such paired models established from the same patient samples, providing detailed insights into how 2D and 3D culture environments drive phenotypic and functional divergence. Despite sharing a patient-of-origin and retaining major oncogenic driver events at the genomic level, these paired models diverged substantially at the phenotypic, transcriptomic, and proteomic levels owing to distinct culture-specific influences. Specifically, our findings demonstrate that PDCs maintain epithelial characteristics, proliferate rapidly, and are well-suited to high-throughput functional analysis, whereas PDOs better preserve tumor 3D architecture, cell–matrix interactions, and microenvironmental complexity, thereby modeling spatial and phenotypic tumor heterogeneity [25,26]. Notably, PDOs frequently exhibited enrichment of ECM components and increased EMT signatures at the protein level, features that correlate with platform-specific resistance to chemotherapy in a patient-dependent manner [27,28]. Collectively, these results highlight that the choice of preclinical model profoundly influences both molecular features and functional phenotypes, including drug response.

https://doi.org/10.5230/jgc.2026.26.e19

jgc Journal of Gastric Cancer

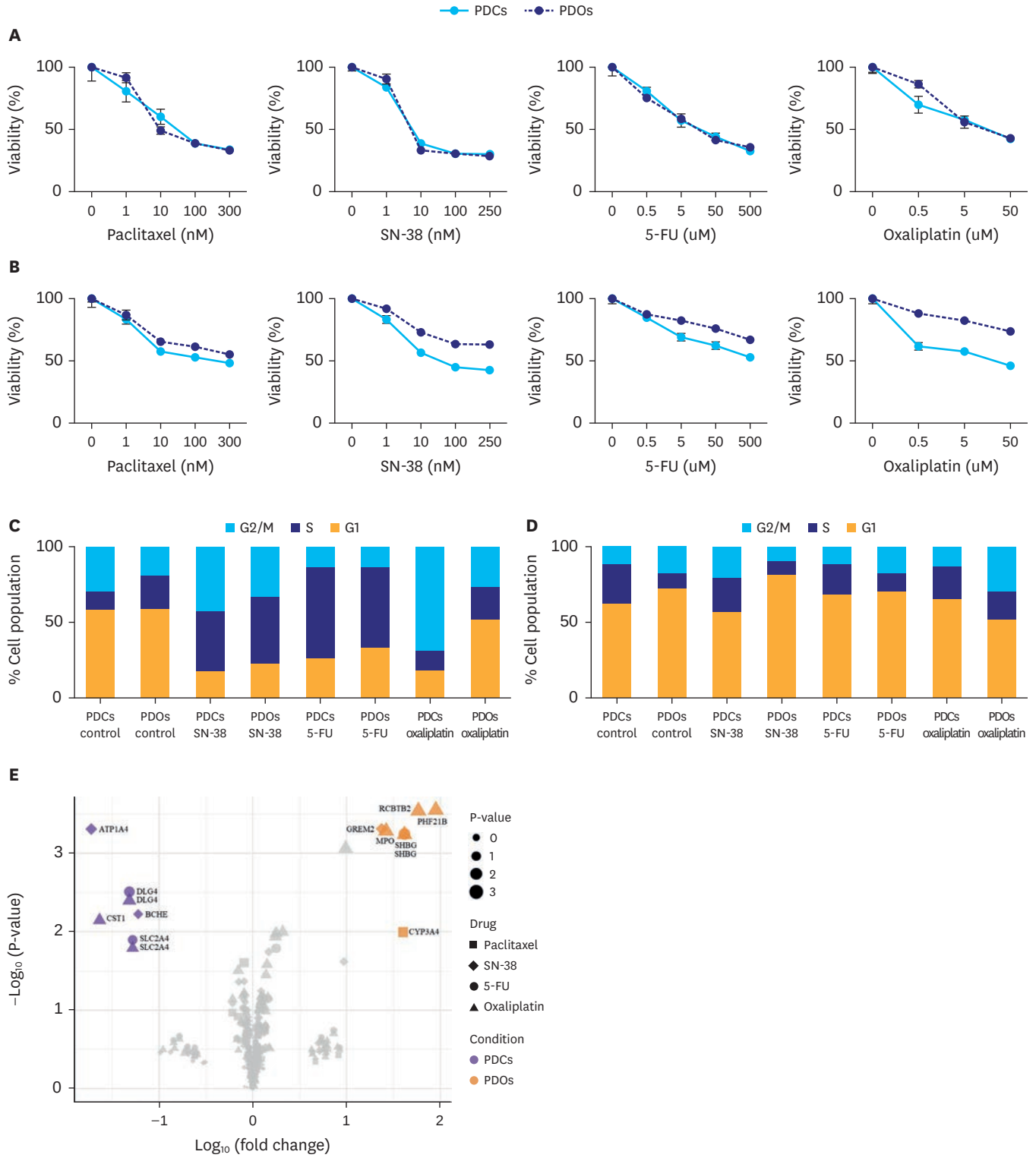

Fig. 6. Profiling of chemotherapeutic drug responses (n=2). (A, B) Dose-response viability curves for YCC-GO10-1 (A) and YCC-GO30 (B) treated with paclitaxel, SN-38, 5-FU, and oxaliplatin. In YCC-GO10-1, PDCs and PDOs show concordant sensitivity to these chemotherapeutic agents, whereas in YCC-GO30, PDOs are comparatively resistant to SN-38, 5-FU, and oxaliplatin. Data are presented as mean ± standard deviation. (C, D) Cell cycle distributions for YCC-GO10-1 (C) and YCC-GO30 (D) following drug treatment. YCC-GO10-1 shows drug-induced cell-cycle arrest with altered phase proportions, whereas YCC-GO30 remains largely unchanged relative to control, consistent with the viability profiles.
5-FU = 5-fluorouracil; PDC = patient-derived cell; PDO = patient-derived organoid.

https://doi.org/10.5230/jgc.2026.26.e19

jgc Journal of Gastric Cancer

Comparison of our results with previous studies confirms that the patient's core genomic alterations, such as ERBB2 amplification and TP53 mutations, are faithfully recapitulated in both models [29]. However, model-specific changes (including subclonal MYC amplification in PDCs or heterogeneous HER2 protein expression in PDOs) suggest that clonal selection and adaptation to the ex vivo environment drive further evolutionary divergence. Importantly, our data show that 3D culture environments, as modeled by PDOs, promote phenotypic heterogeneity and EMT-related protein expression beyond that predicted by genomic status alone. This finding supports the emerging concept that the culture microenvironment, rather than solely the genetic background, is a major determinant of cancer cell state. Functionally, PDCs and PDOs derived from the same patient can have markedly different drug sensitivities. For example, YCC-GO30 PDOs displayed notable resistance to multiple chemotherapeutics compared to paired PDCs, and proteomic analysis revealed a dense ECM signature in these resistant PDOs. These results align with studies suggesting that 3D architecture and ECM remodeling in PDOs confer a microenvironmental barrier to drug penetration and facilitate resistance by activating pro-survival pathways [30]. A key strength of our study is the direct comparison of paired PDCs and PDOs derived from the same tumor source, enabling isolation of the impact of the culture system on tumor biology. However, certain limitations should be acknowledged. The relatively small number of patient samples may restrict the generalizability of our findings. In addition, the lack of matched primary tumors for histopathologic comparison in this ascites-derived cohort precluded assessment of correlations between PDC/PDO morphology and primary tumor histology, an aspect to be addressed in future prospective collections. Although these models mimic many characteristics of the in vivo tumor, they lack critical stromal, immune, and vascular components, which may lead to underestimation of the complexity of drug responses and cellular heterogeneity. Most analyses and functional assays were conducted in vitro, and further in vivo validation, including orthotopic and patient-derived xenograft models, are crucial. Moreover, multi-omics profiling was performed under baseline, drug-naive conditions; thus, these data provide indirect mechanistic context rather than fully capturing the dynamic transcriptional and proteomic changes that occur in response to treatment. Finally, inherent factors such as ECM composition, growth factor conditions, and culture passage number may affect model properties, emphasizing the need for rigorous standardization and transparent reporting to ensure reproducibility across studies. Future studies should prioritize expanding the cohort size across diverse patient backgrounds, integrating co-culture or organ-on-a-chip technologies to better mimic the TME, and performing in vivo functional studies. Prospective evaluation of patient outcomes in relation to in vitro model drug sensitivity will also be essential to establish the predictive and translational value of these platforms. In addition, longitudinal characterization of patient-derived models over extended culture will further clarify their stability and suitability for precision oncology applications.

In conclusion, this direct comparison of paired models demonstrates that the culture system is a major determinant of the cancer cell phenotype, influencing gene expression programs, proteomic landscapes, and therapeutic responses. These findings underscore the importance of selecting context-appropriate models to enhance the translational relevance of preclinical cancer research. Our results further confirm that culture condition, 2D vs. 3D, is a major driver of molecular and functional divergence in patient-derived gastric cancer models, with broad implications for translational studies and therapeutic development. By understanding and addressing the limitations of each model, researchers can more effectively select and apply model systems to answer specific biological and clinical questions.

https://doi.org/10.5230/jgc.2026.26.e19

ACKNOWLEDGMENTS

I would like to thank Editage (www.editage.co.kr) for English language editing.

SUPPLEMENTARY MATERIALS

Supplementary Table 1
Short tandem repeat-based authentication of patient peripheral blood mononuclear cell and corresponding patient-derived models

Supplementary Table 2
Gene list of the CancerMaster targeted sequencing panel (n=524)

Supplementary Table 3
WGS-based copy number of HER2 and MET in PDCs and PDOs

Supplementary Fig. 1
Unsupervised transcriptomic and proteomic analyses. (A, B) PCA of RNA-seq (A) and proteomic (B) data demonstrates clear separation between the 2 culture models. The PCA plots illustrate distinct clustering of PDCs and PDOs based on their respective transcriptomic and proteomic profiles, with variance explained by principal components 1 and 2 indicated on each axis. (C, D) Hierarchical clustering of all genes (C) and all quantified proteins (D) across samples. Heatmaps reveal differential expression of genes and proteins, highlighting model-specific clusters. Transcriptomic data predominantly cluster by culture model (PDCs vs. PDOs), whereas proteomic data cluster primarily by sample, indicating that protein expression may be more influenced by individual patient sample characteristics.

Supplementary Fig. 2
Transcriptomic EMT signature between models. (A, B) Unsupervised hierarchical clustering of transcriptomic data reveals that samples cluster primarily by patient pairs rather than culture model (PDCs vs. PDOs). EMT scores were largely comparable between PDCs and their matched PDOs, indicating limited separation of these models at the RNA level.

Supplementary Fig. 3
Immunohistochemical profiling of HER2, c-MET, CLDN18.2, and EBV in paired PDCs and PDOs. Representative IHC images from 6 patient-derived models (YCC-GO10-1, YCC-GO30, YCC-GO9, YCC-GO58-2, YCC-GO60, and YCC-GO6) are shown for each marker in matched 2-dimensional PDC and 3-dimensional PDO cultures. HER2 staining intensity was scored on a 4-tier scale (0, 1+, 2+, 3+), c-MET and EBV status were classified as positive or negative, and CLDN18.2 expression was quantified as the percentage of positive tumor cells, indicated below each panel. Overall, the staining patterns demonstrate strong pairwise concordance with occasional shifts in intensity or positive fraction, reflecting inter- and intra-model heterogeneity.

Supplementary Fig. 4
Immunohistochemical profiling of EGFR, FGFR2, PD-L1, and TP53 in paired PDCs and PDOs. Representative IHC images from the same 6 patient-derived models are displayed for each marker in corresponding PDC and PDO preparations. EGFR and FGFR2 membrane staining were graded on a 4-tier scale (0, 1+, 2+, or 3+), PD-L1 expression was reported as

jgc Journal of Gastric Cancer

the percentage of positive tumor cells, and TP53 nuclear staining was categorized as 0 (null), 1 (focal positive), or 2 (diffuse positive). These patterns further support preservation of key protein biomarkers between platforms while revealing locus- and marker-specific variation in expression and distribution.

REFERENCES

1. Katt ME, Placone AL, Wong AD, Xu ZS, Searson PC. In vitro tumor models: advantages, disadvantages, variables, and selecting the right platform. Front Bioeng Biotechnol 2016;4:12. PUBMED | CROSSREF
2. Pauli C, Hopkins BD, Prandi D, Shaw R, Fedrizzi T, Sboner A, et al. Personalized in vitro and in vivo cancer models to guide precision medicine. Cancer Discov 2017;7:462-477. PUBMED | CROSSREF
3. Bouchalova P, Bouchal P. Current methods for studying metastatic potential of tumor cells. Cancer Cell Int 2022;22:394. PUBMED | CROSSREF
4. Jeong N, Kim SC, Park JW, Park SG, Nam KH, Lee JO, et al. Multifocal organoids reveal clonal associations between synchronous intestinal tumors with pervasive heterogeneous drug responses. NPJ Genom Med 2022;7:42. PUBMED | CROSSREF
5. Habanjar O, Diab-Assaf M, Caldefie-Chezet F, Delort L. 3D cell culture systems: tumor application, advantages, and disadvantages. Int J Mol Sci 2021;22:12200. PUBMED | CROSSREF
6. Jubelin C, Muñoz-Garcia J, Griscom L, Cochonneau D, Ollivier E, Heymann MF, et al. Three-dimensional in vitro culture models in oncology research. Cell Biosci 2022;12:155. PUBMED | CROSSREF
7. El Harane S, Zidi B, El Harane N, Krause KH, Matthes T, Preynat-Seauve O. Cancer spheroids and organoids as novel tools for research and therapy: state of the art and challenges to guide precision medicine. Cells 2023;12:1001. PUBMED | CROSSREF
8. Hogenson TL, Xie H, Phillips WJ, Toruner MD, Li JJ, Horn IP, et al. Culture media composition influences patient-derived organoid ability to predict therapeutic responses in gastrointestinal cancers. JCI Insight 2022;7:e158060. PUBMED
9. Erali RA, Forsythe SD, Gironda DJ, Schaaf CR, Wajih N, Soker S, et al. Utilizing patient-derived organoids in the management of colorectal cancer with peritoneal metastases: a review of current literature. J Gastrointest Cancer 2023;54:712-719. PUBMED | CROSSREF
10. Park EH, Jung KW, Park NJ, Kang MJ, Yun EH, Kim HJ, et al. Cancer statistics in Korea: incidence, mortality, survival, and prevalence in 2022. Cancer Res Treat 2025;57:312-330. PUBMED | CROSSREF
11. Jung KW, Kang MJ, Park EH, Yun EH, Kim HJ, Kim JE, et al. Prediction of cancer incidence and mortality in Korea, 2025. Cancer Res Treat 2025;57:331-338. PUBMED | CROSSREF
12. Zhao Y, Li S, Zhu L, Huang M, Xie Y, Song X, et al. Personalized drug screening using patient-derived organoid and its clinical relevance in gastric cancer. Cell Rep Med 2024;5:101627. PUBMED | CROSSREF
13. Vistoso Monreal A, Zhao H, Sedghizadeh PP, Lin DC. Patient-derived tumor organoids to model drug response in gastric cancer. Cell Rep Med 2024;5:101650. PUBMED | CROSSREF
14. Duval K, Grover H, Han LH, Mou Y, Pegoraro AF, Fredberg J, et al. Modeling physiological events in 2D vs. 3D cell culture. Physiology (Bethesda) 2017;32:266-277. PUBMED | CROSSREF
15. Muguruma M, Teraoka S, Miyahara K, Ueda A, Asaoka M, Okazaki M, et al. Differences in drug sensitivity between two-dimensional and three-dimensional culture systems in triple-negative breast cancer cell lines. Biochem Biophys Res Commun 2020;533:268-274. PUBMED | CROSSREF
16. Abbas ZN, Al-Saffar AZ, Jasim SM, Sulaiman GM. Comparative analysis between 2D and 3D colorectal cancer culture models for insights into cellular morphological and transcriptomic variations. Sci Rep 2023;13:18380. PUBMED | CROSSREF
17. Kang SK, Bae HJ, Kwon WS, Kim TS, Kim KH, Park S, et al. Inhibition of the bromodomain and extra-terminal family of epigenetic regulators as a promising therapeutic approach for gastric cancer. Cell Oncol (Dordr) 2021;44:1387-1403. PUBMED | CROSSREF
18. Miyoshi H, Stappenbeck TS. In vitro expansion and genetic modification of gastrointestinal stem cells in spheroid culture. Nat Protoc 2013;8:2471-2482. PUBMED | CROSSREF
19. Jung JJ, Jeung HC, Chung HC, Lee JO, Kim TS, Kim YT, et al. In vitro pharmacogenomic database and chemosensitivity predictive genes in gastric cancer. Genomics 2009;93:52-61. PUBMED | CROSSREF
20. Kim E, Kwon WS, Kim TS, Hwang J, Kim S, Rha SY. Identifying anti-cancer effects and exploring the mechanism of an MPS1/TTK inhibitor in gastric cancer. Cancer Res Treat 2025;57:803-820. PUBMED | CROSSREF

21. Subik K, Lee JF, Baxter L, Strzepek T, Costello D, Crowley P, et al. The expression patterns of ER, PR, HER2, CK5/6, EGFR, Ki-67 and AR by immunohistochemical analysis in breast cancer cell lines. Breast Cancer (Auckl) 2010;4:35-41. PUBMED | CROSSREF
22. Kim HJ, Kang SK, Kwon WS, Kim TS, Jeong I, Jeung HC, et al. Forty-nine gastric cancer cell lines with integrative genomic profiling for development of c-MET inhibitor. Int J Cancer 2018;143:151-159. PUBMED | CROSSREF
23. Bae HJ, Kang SK, Kwon WS, Jeong I, Park S, Kim TS, et al. p16 methylation is a potential predictive marker for abemaciclib sensitivity in gastric cancer. Biochem Pharmacol 2021;183:114320. PUBMED | CROSSREF
24. Drost J, Clevers H. Organoids in cancer research. Nat Rev Cancer 2018;18:407-418. PUBMED | CROSSREF
25. Park J, Lee D, Shim JK, Yoon SJ, Moon JH, Kim EH, et al. Mesenchymal stem-like cells derived from the ventricle more effectively enhance invasiveness of glioblastoma than those derived from the tumor. Yonsei Med J 2023;64:157-166. PUBMED | CROSSREF
26. Chang MY, Lee SH. Human pluripotent stem cell-based therapies for Parkinson's disease: challenges and potential solutions. Yonsei Med J 2025;66:395-404. PUBMED | CROSSREF
27. Xing F, Saidou J, Watabe K. Cancer associated fibroblasts (CAFs) in tumor microenvironment. Front Biosci (Landmark Ed) 2010;15:166-179. PUBMED | CROSSREF
28. Seguin L, Desgrosellier JS, Weis SM, Cheresh DA. Integrins and cancer: regulators of cancer stemness, metastasis, and drug resistance. Trends Cell Biol 2015;25:234-240. PUBMED | CROSSREF
29. Tiriac H, Belleau P, Engle DD, Plenker D, Deschênes A, Somerville TDD, et al. Organoid profiling identifies common responders to chemotherapy in pancreatic cancer. Cancer Discov 2018;8:1112-1129. PUBMED | CROSSREF
30. Hahn S, Nam MO, Noh JH, Lee DH, Han HW, Kim DH, et al. Organoid-based epithelial to mesenchymal transition (OEMT) model: from an intestinal fibrosis perspective. Sci Rep 2017;7:2435. PUBMED | CROSSREF